Catalysis Letters, Vol. 113, Nos. 3–4, February 2007 (© 2007)
DOI: 10.1007/s10562-007-9023-y

Oxidative dehydrogenation of *n*-butane over mesoporous VO_x/SBA-15 catalysts

Wei Liu,[a] Suk Yin Lai,[a] Hongxing Dai,[a,b] Shuiju Wang,[c] Haizhen Sun,[c] and Chak Tong Au[a,*]

[a]*Department of Chemistry, Centre for Surface Analysis and Research, Hong Kong Baptist University, Kowloon Tong Hong Kong, China*
[b]*Department of Chemistry and Chemical Engineering, College of Environmental and Energy Engineering, Beijing University of Technology, Beijing 100022, China*
[c]*Chemistry and Chemical Engineering College, Xiamen University, Xiamen 361005, China*

Received 15 October 2006; Accepted 1 December 2006

Mesoporous VO_x/SBA-15 catalysts with different V contents were evaluated for the oxidative dehydrogenation of *n*-butane and characterized by N_2 adsorption, XRD, HRTEM, H_2-TPR, NH_3-TPD, XPS, and EPR techniques. Compared to conventional V_2O_5/SiO_2 catalysts, the VO_x/SBA-15 catalysts showed better performance. The good performance can be attributed to the good dispersion of V species, presence of V^{4+} species and the pore structure.

KEY WORDS: mesoporous SBA-15; vanadium oxide; oxidative dehydrogenation; *n*-butane.

1. Introduction

The oxidative dehydrogenation (ODH) of *n*-butane to butenes and butadiene offers an attractive route for the production of olefins. The ODH reaction is thermodynamically feasible and is not limited by equilibrium [1]. It possesses many advantages: it is exothermic, irreversible, and can proceed at temperatures lower (by ca. 200 °C) than that required for the non-oxidative pyrolysis process. The ODH approach can limit coke formation and thermal cracking of products, and hence can prolong the life span of the catalysts [2]. The ODH of *n*-butane has been extensively studied since 1967 and discussed in several review papers [e.g., 3–5]. However, the ODH of *n*-butane is still far from being attractive for industrial applications because the overall combustion of *n*-butane, butenes and butadiene leads to low selectivity, especially at high *n*-butane conversion. Indeed the design of a catalyst that gives a high C_4-olefins yield for this reaction is still a challenge.

It has been reported that V_2O_5 supported on SiO_2 [6–9], Al_2O_3 [10,11], and MgO [12–14] are catalytically active for the ODH of light alkanes for alkene generation. It is generally accepted that the dispersion of V_2O_5 and the nature of support have great influence on both alkane conversion and alkene selectivity. Kung *et al.* [6] studied the effect of vanadia loading on silica for the ODH of *n*-butane. The results showed that the well-dispersed vanadia (0.58 wt% vanadium loading) catalyst was more selective than the one (6.4 wt% vanadium loading) with crystalline V_2O_5 formation.

*To whom correspondence should be addressed.
E-mail: pctau@hkbu.edu.hk

Mesoporous molecular sieves M41S can provide more room for the dispersion of vanadia and hence generating more active sites [15–18]. Solsona *et al.* [16] reported that compared with amorphous silica, the use of MCM-41 as support resulted in higher concentration of isolated tetrahedral vanadium species and greater density of active sites. As a result, the VO_x/MCM-41 catalysts showed higher olefins yield in the ODH of propane and ethane.

Using a triblock copolymer as template, Zhao *et al.* [19] generated the mesoporous SBA-15, which possess structures more regular and channel walls much thicker than those of MCM-41. The pore size of SBA-15 can be controlled and the pores are well-defined. The SBA-15 materials are thermally stable and of high surface areas. With these unique properties, SBA-15 has been investigated as catalyst support for reaction such as *n*-butane oxidation to maleic anhydride [20], selective photo-assisted oxidation of methane to formaldehyde [21], and partial oxidation of methane to formaldehyde [22]. Hess *et al.* [23] prepared VO_x/SBA-15 using grafting/anion-exchange procedure and characterized the catalysts by Raman and UV–vis spectroscopy. The results showed that at vanadium loading of up to 7.2 wt%, the vanadia species are isolated whereas at higher loadings V_2O_5 crystallites are formed in addition to the monomeric and polymeric vanadia species. Fan and coworkers used VO_x/SBA-15 as catalysts for the ODH of propane [24, 25]. They found that catalytic activity over VO_x/SBA-15 is higher than that of V_2O_5/MCM-41 and attributed the enhanced performance to the particularly larger pore size and lower surface acidity of the former. In another work, Hess *et al.* [26] adopted a

preparation procedure similar to that proposed in Ref. [23] to obtain the nanostructured SBA-15-supported vanadia catalysts and found that these materials exhibited high selectivity to acrylic acid in the partial oxidation of propane.

With large pore size, the SBA-15 materials permit easy diffusion of gaseous molecules inside the pore channels. With the anchoring of VO_x species onto the inner walls of the mesopores, there is good accessibility of reactant gas to the active sites and rapid departure of the desired products. In this work, we prepared VO_x/SBA-15 of different VO_x loadings and investigated for the first time the catalytic activity of VO_x/SBA-15 catalysts for the ODH of *n*-butane.

2. Experimental

2.1. Catalyst preparation

The SBA-15 was synthesized according to the procedure described by Zhao *et al.* [19]. In a typical synthesis, 2.0 g triblock poly(ethylene oxide)-poly (propylene oxide)-poly(ethylene oxide) ($EO_{20}PO_{70}EO_{20}$, P123, Aldrich) was dissolved in 60 g deionized water, and 11.8 g HCl (37%, Aldrich) was added with stirring. Then 4.4 g tetraethyl orthosilicate (TEOS, 98%, aldrich) was added to the solution at 40 °C. After being stirred for 24 h, the mixture was transferred to an autoclave and placed in an oven at 90 °C for 48 h. The precipitate was filtered and then washed with deionized water and acetone, respectively, before being dried at room temperature (RT) and calcined in air at 600 °C for 5 h, with a ramp rate of 1 °C/min.

The loading of VO_x (2.24–28.0 wt% V content) on SBA-15 was by means of incipient wetness impregnation of SBA-15 with a solution of ammonium metavanadate and oxalic acid (molar ratio 1:2) as described by Dai *et al.* [11]. First, the required amount of ammonium metavanadate (99%, Aldrich) and corresponding amount of oxalic acid dihydrate (99%, Aldrich) were dissolved in 4 mL deionized water. Then 1.0 g of SBA-15 powder was added and the mixture was dried at 120 °C overnight. The dried precursor was heated from RT to 500 °C at a rate of 1 °C/min and kept at this temperature for 6 h in air. The samples are denoted as *x*V-SBA-15, where *x* represents the V weight percentage in the calcined catalysts. For comparison, a V_2O_5/Aerosil catalyst with 8.96 wt% V content was also prepared. This catalyst is named as 8.96V-SiO_2. In the synthesis, the fumed silica Aerosil 200 (Degussa, surface area = 187 m^2/g) was first treated with deionized water and dried at 120 °C overnight before being subject to similar treatment for VO_x impregnation. The weight percent of vanadium for all the catalysts are calculated relative to the weight of the support.

2.2. Catalyst characterization

The BET surface areas and pore size distributions of the samples were measured by means of a Quantachrome NOVA-1200 instrument. The samples were degassed at 300 °C for 3 h before the adsorption of N_2 at −196 °C. Powder X-ray diffraction investigation was conducted using a Rigaku diffractometer (Rigaku D-MAX) with Ni filtered Cu $K\alpha$ radiation. The morphology of the catalyst was examined via the use of a FEI TECNAI Field Emission HRTEM. The XPS investigation was conducted using a spectrometer equipped with a VG CLAM 4 MCD Analyzer and Mg-$K\alpha$ (1253.6 eV) radiation. The binding energies (BEs) were calibrated against the C1s signal (284.6 eV) of contaminant carbon. The surface concentrations of elements were estimated on the basis of the corresponding peak areas being normalized using the Wagner Factor database.

H_2 temperature-programmed reduction (H_2-TPR) was carried out in the 100–900 °C range. Samples (50 mg) were treated in dry air at 500 °C for 1 h and then cooled down to RT in N_2 flow (50 mL/min) before being reduced in a flow of 5% H_2/Ar (50 mL/min) at a ramping rate of 10 °C/min. The effluent was monitored with a TCD detector. NH_3 temperature-programmed desorption (NH_3-TPD) was performed on the same instrument. The sample was pretreated in a flow of dry air (30 mL/min) at 500 °C for 1 h. Then the sample was exposed to NH_3 at RT for 30 min. After N_2 purging of the sample (to remove gas-phase NH_3) for 1 h, TPD was performed in N_2 flow (50 mL/min) at a heating rate of 10 °C/min, and the desorbed NH_3 was monitored by a TCD detector.

Samples after various treatments were transferred to a JEOL JES-TE100 ESR spectrometer operating in X-band without being exposed to air. The EPR spectra were recorded at RT; microwave power was 1.17 mW with a resonance frequency of ca. 9.44 GHz at 100 kHz modulation. The tube for EPR measurement is shown in Scheme 1. The sample was first treated in Treatment Tube. After treatment, the sample was cooled to room temperature in the treatment gas. With the sealing of gas inlet and outlet and the turning (90° anticlockwise) of

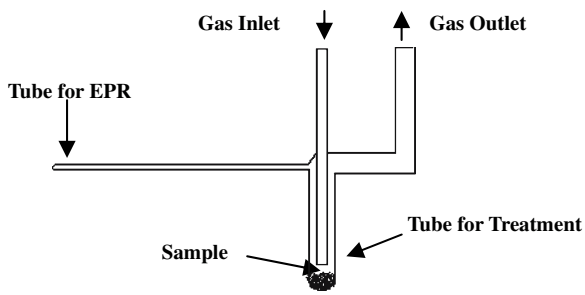

Scheme 1. Sample tube for EPR measurement.

the tube assembly, the treated sample was transferred to the Measurement Tube for EPR analysis.

2.3. Catalytic test

The ODH of *n*-butane was carried out in a quartz microreactor at atmospheric pressure at a feed gas ($C_4H_{10}/O_2/N_2$ = 4:8:88) flow rate of 100 ml/min. Unless specified otherwise, the amount of catalyst for each test was 0.2 g. A thermocouple was placed in the middle of the catalyst bed to measure the reaction temperature. The effluent was analyzed on-line by using a GC system (Shimadzu 8A). One GC equipped with FID detector and 0.19% picric acid/Carbograph column was used to separate hydrocarbons. The other one equipped with TCD and columns of Porapak Q and molecular sieve 5A was used to detect CO, CO_2 and O_2. Conversion of *n*-butane and selectivity to products were calculated based on the balance of carbon.

3. Results and discussion

3.1. Characterization

3.1.1. Textural properties

Figure 1 gives the pore size distributions of SBA-15 and VO_x/SBA-15. The related data are summarized in table 1. As depicted in table 1, SBA-15 has high surface area (881 m^2/g), large average pore diameter (51.3 Å), and large pore volume (1.13 mL/g). The loading of VO_x on SBA-15 resulted in decreases in surface area and pore volume. It is obvious that the surface area of 8.96V-SBA-15 was much larger than that of 8.96 V-SiO_2. The surface density for a nominal monolayer is about 6.6 V/nm^2. Except for the 8.96V-SiO_2 and 28.0 V-SBA-15 samples, the surface concentration of vanadium remained in the sub-monolayer region.

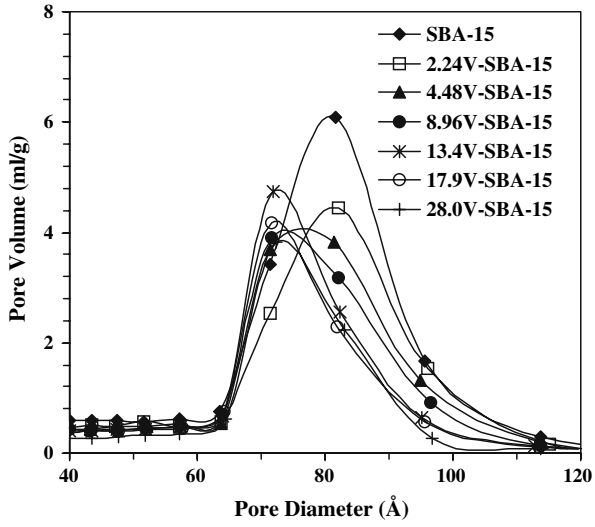

Figure 1. Pore size distributions of *x*V-SBA-15 catalysts.

SBA-15 and all the VO_x/SBA-15 catalysts showed type IV isotherms with a sharp increase in gas-uptake volume in the P/P_0 range of 0.5–0.8, typical of mesoporous structures with well-defined pores. Compared with SBA-15, the VO_x/SBA-15 catalysts are narrower in pore size distribution (figure 1). At V content higher than 4.48 wt%, the pore size of the catalysts deviates from that of SBA-15 and shifts to lower values. At 2.24 wt% V content, the amount of VO_x in the pores is low enough not to cause obvious change in pore size. At 4.48 wt% V content, with more VO_x species anchored on the walls of the SBA-15 mesopores, there was a reduction in pore size (from 81.6 to 76.5 Å). At 8.96 wt% V content, the mesopore size was further reduced to 73.0 Å. From 8.96 to 28.0 wt% V content, there was little change in pore size. The result suggests that addition of vanadium within this range does not lead to a growth in the thickness of V clusters within the mesopores but the further deposition would cause the formation of larger particle outside the mesopores. In general, we observed that with an increase in VO_x loading, there is a gradual increase in average pore diameter. The phenomenon is attributed to the blocking of micropores that branch out from the SBA-15 mesopores. The very fact that the average pore diameter (51.3 Å) is smaller than the mesopore diameter (81.6 Å) is a proof of the existence of micropores in SBA-15 [20,27,28].

The HRTEM images of SBA-15, VO_x/SBA-15 with 2.24 and 8.96 V content are shown in figure 2. The highly ordered array of mesoporous channels of these samples can be seen clearly. The TEM images reveal that the ordered mesoporous structure of SBA-15 is preserved after it is loaded with vanadium oxide.

3.1.2. XRD

The small-angle XRD patterns of SBA-15 and VO_x/SBA-15 with V content below 13.4 wt% show three well-resolved Bragg peaks at 2θ = 0.90, 1.75, and 2.08°, attributable to (100), (110), and (200) diffraction, respectively. These peaks are characteristics of the hexagonal ordered structure of SBA-15 [19]. With further rise in VO_x loading, the (100) peak weakens in intensity and gradually disappeared, a result of the partial blocking of SBA-15 mesopores (by VO_x) and the decline in long-range order of hexagonally arranged porosity. The (110), and (200) diffraction peak can still be detected at 28.0 wt% V content. In other words, the SBA-15 pore structure is retained in the prepared VO_x/SBA-15 catalysts.

In the wide-angle XRD study, we observed no peaks of crystalline V_2O_5 below 13.4 wt% V content, indicative of good VO_x dispersion on SBA-15. At or above 13.4 wt% V content, peaks of crystalline V_2O_5 appeared. These results are in agreement with the data of surface area and pore size distribution. Above 13.4 wt% V content, the specific surface area decreased rapidly. With the accumulation of VO_x on the external

Table 1
Physical properties of SBA-15, *x*V-SBA-15, and V_2O_5/Aerosil 200

Sample	V surface density (V/nm^2)	S_{BET}(m^2/g)	Pore volume (mL/g)	Mesopore diameter(Å)	Average pore diameter (Å)
SBA-15	–	881	1.13	81.6	51.3
8.96V-SiO_2	7.42	123	–	–	–
2.24V-SBA-15	0.38	674	0.88	81.0	52.3
4.48V-SBA-15	0.78	632	0.84	76.5	53.0
8.96V-SBA-15	1.69	540	0.76	72.0	56.1
13.4V-SBA-15	2.48	516	0.74	71.0	56.9
17.9V-SBA-15	3.88	414	0.64	71.0	61.5
28.0V-SBA-15	7.80	283	0.51	71.0	72.7

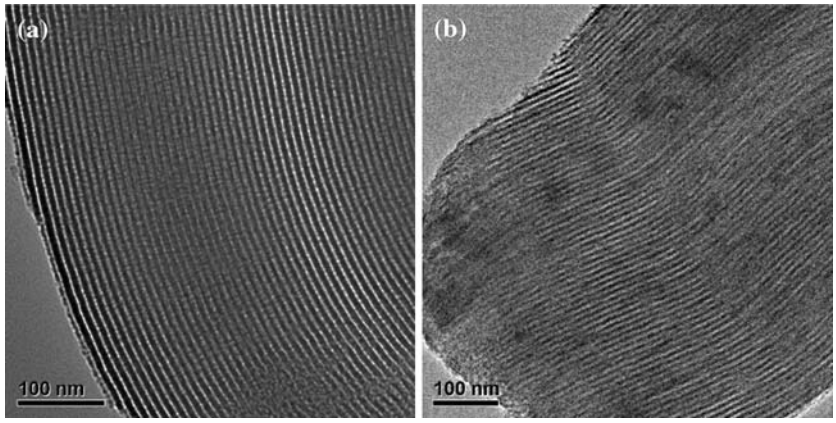

Figure 2. TEM images of (a, b) parent SBA-15, (c) 2.24V-SBA-15, and (d) 8.96V-SBA-15.

surface of SBA-15, VO_x aggregates to form V_2O_5 crystallites, blocking some of the pore mouths leading to both decrease in specific surface area and pore volume. Since SiO_2 has much lower surface area than SBA-15, V_2O_5 crystallites formed at lower loading were detected over 8.96 V-SiO_2.

3.1.3. XPS

The XPS results of the catalysts are summarized in table 2. The $V2p_{3/2}$ BEs of VO_x/SBA-15 are in the range of 516.4–516.8 eV, lower than that of V_2O_5 (517.4 eV) reported in the literature [29]. It is clear that the oxidation state of vanadium in the catalysts is below 5+, i.e., there is certain amount of V^{4+} in the samples. By deconvolution, two components at 516.1 and 517.1 eV are obtained under the $V2p_{3/2}$ profile, the former is assigned to V^{4+} whereas the latter to V^{5+} (figure 3). The percentage of V^{5+} and V^{4+} to total V species are depicted in table 2. One can see that there is a decrease in V^{4+} but a rise in V^{5+} content with increasing loading of vanadium. During the preparation of VO_x/SBA-15, the precursor of VO_x (NH_4VO_3) first formed VO_2^+ in the acidic solution. Then the VO_2^+ species was reduced to VO^{2+} species by oxalic acid. The good stability of SBA-15 and the accommodation of V^{4+} species inside the SBA-15 matrix favor the retention of tetravalent vanadium. At or above 13.4 wt% V content, with the aggregation of the vanadium species and the formation of V_2O_5 crystallites on the surface of SBA-15, there is the conversion of V^{4+} to V^{5+}.

The O1s BEs are in the 532.8–533.0 eV range, much higher than that of V_2O_5 (530.2 eV) but close to that of SBA-15 (533.0 eV). So the O1s signals of the catalysts are mainly from SBA-15. Only very weak O1s signal of V_2O_5 is detected at high VO_x loadings, suggesting that most of the loaded VO_x species are inside the pores.

The surface composition and the surface V/Si atomic ratios calculated based on $V2p_{3/2}$ and Si2p peak areas and atomic sensitivity factors are listed in table 2. As shown in figure 4, the slope of the V/Si ratio against V content plot between 2.24 and 8.96 wt% is larger than that between 13.4 and 28.0 wt%. The results give a clear indication that above 8.96 wt%, there is a decline in VO_x dispersion on the external surface of SBA-15 due to VO_x aggregation. For the sake of comparison, the V/Si atom ratios of *x*V-SBA-15 based on bulk composition are also included in table 2. The V/Si atom ratios of bulk composition are much larger than that of XPS results. It is because the vanadium species anchored on the inner walls of the pores are undetectable by the XPS technique, which is surface sensitive.

3.1.4. H_2–TPR

In H_2-TPR results, reduction of the supported samples occurred within the 340–650 °C range, much lower

Table 2
XPS results of SBA-15, V_2O_5, and xV-SBA-15 catalysts

	$V2p_{3/2}$(eV) (percentage of V^{4+} and V^{5+})	O1s (eV)	Surface composition (at%)			V/Si[b]	V/Si[c]
			V	O	Si		
SBA-15	–	533.0	–	–	–	–	–
V_2O_5[a]	517.4	530.2	–	–	–	–	–
2.24V-SBA-15	516.1 (82.4%) 517.1 (17.6%)	533.0	0.14	77.0	22.9	0.006	0.026
4.48V-SBA-15	516.1 (70.2%) 517.1 (29.8%)	532.8	0.36	77.7	22.0	0.016	0.057
8.96V-SBA-15	516.2 (42.8%) 517.1 (57.2%)	533.0	0.95	78.9	20.1	0.047	0.106
13.4V-SBA-15	516.1 (26.4%) 417.1 (73.6%)	533.0	1.24	76.6	22.1	0.056	0.158
17.9V-SBA-15	516.2 (3.8%) 517.2 (96.2%)	533.0	1.26	77.8	21.0	0.060	0.211
28.0V-SBA-15	516.1 (2.3%) 517.1 (97.7)	532.8	1.64	78.3	19.8	0.083	0.330

[a]From Ref. [29]. [b]Based on XPS results. [c]Based on bulk composition.

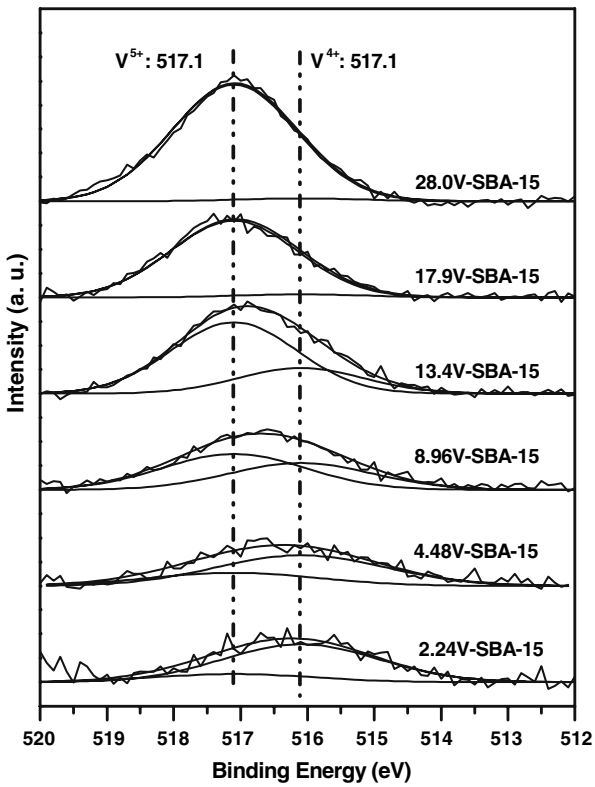

Figure 3. Deconvolution of $V2p_{3/2}$ signals of xV-SBA-15.

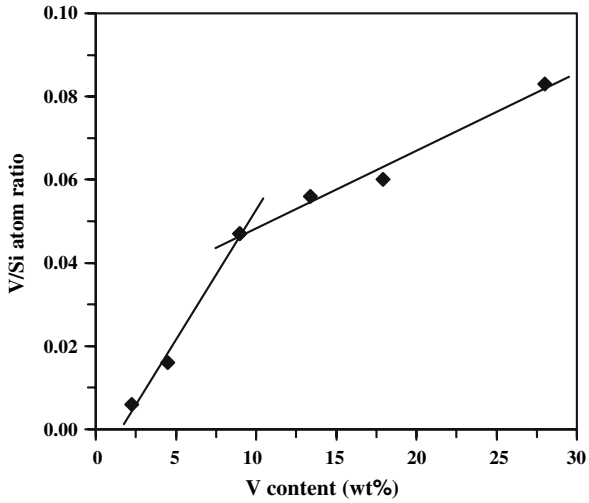

Figure 4. Plot of V/Si atomic ratio versus V content based on the data in table 2.

than the reduction range of V_2O_5 which is above 660 °C. There was a reduction peak at around 450 °C on all the V-SBA-15 catalysts. Comparing the results with those of V_2O_5/SiO_2 reported by Arena *et al.* [30], we assign the 450 °C peak to the reduction of surface V ions with unsaturated coordination. It is clear that due to the promoted dispersion of VO_x species in the mesopores of SBA-15, there is enhanced amount of V ions of unsaturated coordination anchored on the pore walls. For the samples with V content ranging from 2.24 to 8.96 wt%, there was a reduction peak at ca. 546 °C. This peak became dominant at 4.48 wt% V content and shifted gradually from 546 to 589 °C within the 8.96–28.0 wt% range, and one can see that there is a gradual development of a shoulder at about 615 °C. The peak at 546 °C can be attributed to the reduction of well dispersed tetrahedral vanadium species [30]. The progressive shift of the major H_2 consumption peak to higher temperature with loading rise is due to the gradual formation of polymeric vanadium species [31–34]. The shoulder peaks at 615 °C and 665 °C on catalysts with high V content are due to the step-wise reduction of V_2O_5 crystallites. The presence of V_2O_5 crystallites has been proved by the wide-angle XRD results.

3.1.5. NH_3-TPD

The NH_3-TPD results are shown in figure 5. There is a weak peak at 77 °C over SBA-15 which may be related to the NH_3 adsorbed at very weak acidic sites. Over the VO_x/SBA-15 samples, there are two NH_3 desorption peaks partially overlapping in the 70–250 °C range. With rise in VO_x loading, there is a rise in peak intensity, and the position of the second component shifts to higher temperatures. The results suggest that there are two kinds of acidic sites and with rise in VO_x loading, the catalysts become more acidic. The results are different from those reported by Fan *et al.* [24]. They observed no NH_3-TPD peaks over SBA-15 whereas over VO_x/SBA-15 they detected a wide peak at 205–220 °C. Such discrepancies can be due to the difference in ammonia adsorption temperature.

3.1.6. EPR

The EPR characterization of the as-prepared 8.96V-SBA-15 sample and the sample after different treatments were carried out at RT. The as-prepared 8.96V-SBA-15 catalyst shows one axially symmetric signal with hyperfine splitting. The hyperfine splitting is originated from the magnetic interactions between magnetic moments of the unpaired $3d^1$ electron of vanadium and the magnetic atomic ^{51}V nuclei ($I = {}^7/_2$, natural abundance, 99.75%). The signal can be attributed to VO^{2+} species because V^{5+} is silent to EPR. For the sample treated in air at 500 °C for 1 h, there is a significant reduction in VO^{2+} intensity due to the conversion of VO^{2+} to V^{5+}. After reduction in H_2 at 500 °C for 1 h, the 8.96V-SBA-15 sample showed well-resolved hyperfine signals similar to those of the as-prepared sample. The enhanced signal intensity of VO^{2+} species reflects the reduction of V^{5+} to VO^{2+} species. The reduction of V^{5+} to V^{4+} species during ODH of alkanes has been reported by Brückner *et al.* [35]. The reduction of V^{5+} to V^{4+} during the ODH of *n*-butane can be seen clearly in the spectrum of the sample treated in reaction gas at 500 °C for 1 h. Due to the increased concentration of VO^{2+}, the signal of VO^{2+} is strong.

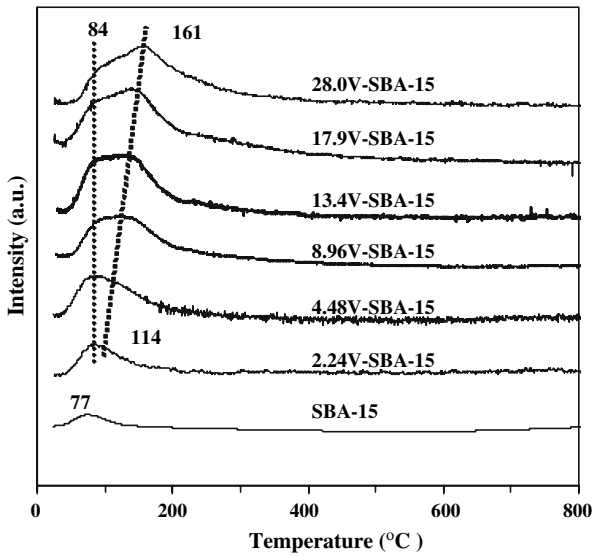

Figure 5. NH_3-TPD profiles of SBA-15 and *x*V-SBA-15.

3.2. Catalytic activity

The ODH reactions of *n*-butane with oxygen over the VO_x/SBA-15 catalysts yield ethene and ethane (C_2), propene and propane (C_3), *iso*-butene and butane (*i*-C_4), 1-butene (1-C_4), *cis*- and *trans*-2-butene (*c*−C_4 and *t*−C_4), 1,3-butadiene (1,3-C_4) and carbon oxides (CO_x, i.e., CO and CO_2). Pure SBA-15 also shows certain ODH activity with 12.7% selectivity to C_4-olefins at 13.7% *n*-butane conversion at 520 °C and a space velocity of 30,000 $cm^3h^{-1}g^{-1}{}_{cat}$. As reported by Owens and Kung [6], V_2O_5 and 0.53 wt% V/Cabosil silica show a *n*-butane conversion of 11.0 and 22.8%, and C_4-olefins selectivity of 7 and 46%, respectively. The 8.96V-SiO_2 studied here with much higher V content showed significantly higher conversion (47.8%) but lower C_4-olefins selectivity (15.6%). Compared with V_2O_5/SiO_2,VO_x/SBA-15 showed much higher catalytic performance in the ODH of *n*-butane. From table 3, one can find that higher conversion and selectivity are obtained when the V content of VO_x/SBA-15 is below 13.4 wt%. The conversion and selectivity first increases and then decreases with the rise in V content, reaching a maximum value at 4.48 and 8.96 wt%, respectively. At 4.48 and 8.96 wt% V content, the catalysts give a maximum yield of ca. 15% under the adopted reaction conditions. According to Mamedov and Cortés Corberán [5], isolated monovanadate is more selective than polyvanadate (i.e., polymeric vanadate). That is to say, the latter is more active but less selective. But in a reaction of restricted supply of oxygen, there is enhancement in butene selectivity and in *n*-butane conversion because ODH reaction consumes less oxygen than deep oxidation to CO_x. When the vanadia loading is over one monolayer, crystalline V_2O_5 appears (XRD and TPR results), resulting in decrease in both conversion and selectivity.

Blasco *et al.* [36] found that selectivity to dehydrogenation products as well as distribution of C_4-olefins can be related to the acid-base character of the catalysts. We observed that the distribution of products depends on the physico-chemical properties of the VO_x/SBA-15 catalysts, especially on the vanadium species and the acid–base property. It has been reported that 1-butene and butadiene selectivity decreased when the strength and number of acid sites increased, while selectivity to 2-butene and CO_x showed the opposite trend [36]. It is generally accepted that on crystalline V_2O_5 *n*-butane is more likely to undergo deep oxidation to produce CO_x. Similar trends were observed in our results

Table 3
Catalytic performance of V_2O_5, SBA-15, and xV-SBA-15 at 520 °C and a space velocity of 30,000 $cm^3\ h^{-1}\ g^{-1}_{cat}$

Catalyst	Conv. (%)	Selectivity (%)									Dehy. yield[c] (%)
		CO	CO_2	C_2/C_3	i-C_4	1-C_4	c-C_4	t-C_4	1,3-C_4	Dehy.[b]	
V_2O_5[a]	11.0	34.0	58.0	0	0	7.0	0	0	0	7.0	0.8
SBA-15	13.7	57.0	18.0	11.1	0.5	5.8	2.1	3.9	0.9	12.7	1.7
8.96V-SiO_2	47.8	58.3	22.8	3.3	0	3.6	3.9	5.2	2.9	15.6	7.5
2.24V-SBA-15	44.4	51.6	13.0	2.8	7.1	10.9	4.1	4.9	5.7	25.6	11.4
4.48V-SBA-15	57.1	54.0	10.9	5.3	2.6	7.6	4.1	4.7	10.0	26.4	15.1
8.96V-SBA-15	54.8	56.1	11.7	3.9	1.2	5.7	5.5	6.9	9.2	27.3	15.0
13.4V-SBA-15	48.2	62.1	16.4	3.5	0.2	3.9	3.9	5.2	3.7	16.7	8.0
17.9V-SBA-15	43.3	70.8	16.1	2.1	0.2	2.2	2.8	2.9	1.1	9.0	3.9
28.0V-SBA	27.3	66.0	19.8	1.7	0.3	3.2	2.8	4.9	0.6	11.5	3.1

[a]From Ref. [6].
[b] linear C_4 alkene selectivity.
[c]linear C_4 alkene yield.

(table 3). The overall selectivity to 1-butene and 1,3-butadiene over the 28.0V-SBA-15 catalyst was much lower than that over the 2.24V-SBA-15. As shown in table 3, CO_x selectivity increased obviously with the rise in V content: CO_x selectivity was 64.6% at 2.24 wt% V content and became 85.8% at 28.0 wt% V content.

At a *n*-butane concentration of 4% and a *n*-butane to oxygen ratio of 1/2, we investigated the effect of reaction temperature (460–540 °C) on the catalytic activity over the 8.96V-SBA-15 catalyst (figure 6). The conversion of *n*-butane varied slightly within a narrow range of 51–58%. The decline in *n*-butane conversion above 480 °C could be related to the reduction in the amount of V^{5+} as revealed by the EPR results, which showed that during the reaction some of the V^{5+} species were reduced to V^{4+} species. Another possible reason is that a certain amount of active sites had been covered by the carbon formed during reaction. The increase-and-then-decrease trend of selectivity is clear, and the best yield was achieved at 520 °C. The significant decreases in selectivity and yield above 520 °C is due to the cracking and deep oxidation of olefins to by-products.

At reaction temperature of 520 °C and *n*-butane feed concentration of 4%, we investigated the effect of contact time on the catalytic activity of 8.96V-SBA-15 (figure 7). One can see that the conversion increased linearly with the rise in contact time, reflecting the irreversible nature of the reaction [2]. The selectivity and yield passed through a maximum at contact time of 18.7 $g_{cat}\ h\ mol_{c4}^{-1}$. Above 18.7 $g_{cat}\ h\ mol_{c4}^{-1}$, the decline in selectivity and yield was a result of enhanced olefins conversion to cracking products and carbon oxides.

4. Conclusion

Mesoporous VO_x/SBA-15 catalysts with 2.24–28.0 wt% V content have been prepared by incipient wetness impregnation and characterized by a number of

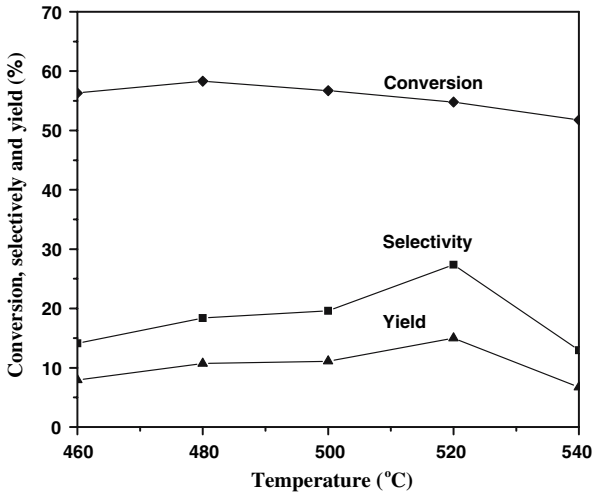

Figure 6. *n*-Butane conversion, C_4-olefin selectivity, and C_4-olefin yield over 8.96V-SBA-15 as a function of temperature.

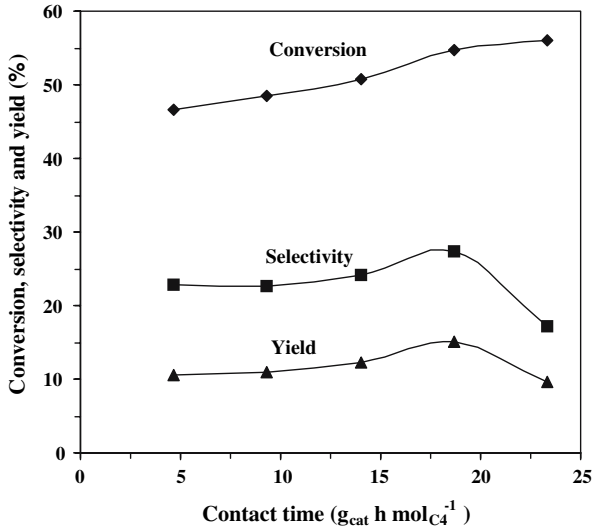

Figure 7. *n*-Butane conversion, C_4-olefin selectivity, and C_4-olefin yield over 8.96V-SBA-15 as a function of contact time.

techniques for the ODH reaction of *n*-butane. According to the results of XRD and H_2-TPR investigations, at or below 8.96 wt% V content, the VO_x species show good dispersion and spread on the wall of pore channels as well as on the external surface of SBA-15. At loadings higher than 8.96 wt% V content, VO_x species aggregate and V_2O_5 crystallites are formed on the external surface of SBA-15.

The catalytic selectivity can be related to the extent of the vanadium deposition and acidic nature of the catalysts. With the rise of acidity at higher loadings, there is a drop in 1-butene and 1,3-butadiene selectivity but a rise in CO_x selectivity. Compared to 8.96V-SiO_2, the 8.96V-SBA-15 catalyst showed significantly higher *n*-butane conversion and C_4-olefins selectivity. Relating the EPR and XPS results with the performance of the catalysts, it is apparent that V^{4+} has a role to play. Despite V^{4+} is less active than V^{5+}, the former can lower the vanadium redox potential and is more selective than the latter for butenes formation. Over VO_x/SBA-15 catalyst with 4.48 wt% and 8.96 wt% V content, C_4-olefin yield is ca. 15% at 520 °C, much higher than the maximum yield (10.4%) reported over conventional V_2O_5/SiO_2 catalysts.

Acknowledgments

The work was supported by the Research Grants Council of the Hong Kong Special Administration Region (Grant No. HKBU 200103); the research activities conducted in BJUT was financed by the National Natural Science Foundation of China (Grant No. 20473006).

References

[1] M.A. Chaar, D. Patel and H.H. Kung, J. Catal. 109 (1988) 463.
[2] D. Bhattacharyya, S.K. Bej and M.S. Rao, Appl. Catal. 87 (1992) 29.
[3] L.M. Madeira and M.F. Portela, Catal. Rev.-Sci. Eng. 44 (2002) 247.
[4] T. Blasco and J.M. López Nieto, Appl. Catal. A 157 (1997) 117.
[5] E.A. Mamedov and V. Cortés Corberán, Appl. Catal. A 127 (1995) 1.
[6] L. Owens and H.H. Kung, J. Catal. 144 (1993) 202.
[7] S. Ted Oyama and G.A. Somorjai, J. Phys. Chem. 94 (1990) 5022.
[8] A. Erdöhelyi and F. Solymosi, J. Catal. 123 (1990) 31.
[9] A. Erdöhelyi and F. Solymosi, J. Catal. 129 (1991) 497.
[10] T. Blasco, A. Galli and J.M. López Nietó, J. Catal. 169 (1997) 203.
[11] H.X. Dai, A.T. Bell and E. Iglesia, J. Catal. 221 (2004) 491.
[12] M.A. Chaar, D. Patel, M.C. Hung and H.H. Kung, J. Catal. 105 (1987) 483.
[13] A.A. Lemonidou, G.J. Tjatjopoulos and I.A. Vasalos, Catal. Today 45 (1998) 65.
[14] R. Vidal-Michel and K.L. Hohn, J. Catal. 221 (2004) 127.
[15] Q.H. Zhang, Y. Wang, Y. Ohishi, T. Shishido and K. Takehira, J. Catal. 202 (2001) 308.
[16] B. Solsona, T. Blasco, J.M. López Nieto, M.L. Peña, F. Rey and A. Vidal-Moya, J. Catal. 203 (2001) 443.
[17] P. Selvam and S.E. Dapurkar, J. Catal. 229 (2005) 64.
[18] K.J. Chao, C.N. Wu and H. Chang, J. Phys. Chem. B 101 (1997) 6341.
[19] D.Y. Zhao, J.L. Feng, Q.S. Huo, N. Melosh, G.H. Fredrickson, B.F. Chmelka and G.D. Stucky, Science 279 (1998) 548.
[20] X.K. Li, W.J. Ji, J. Zhao, Z.B. Zhang and C.T. Au, J. Catal. 238 (2006) 232.
[21] H.H. López and A. Martínez, Catal. Lett. 83 (2002) 37.
[22] V. Fornés, C. López, H.H. López and A. Martínez, Appl. Catal. 249 (2003) 345.
[23] C. Hess, J.D. Hoefelmeyer and T. Don Tilley, J. Phys. Chem. B 108 (2004) 9703.
[24] Y.M. Liu, Y. Cao, S.R. Yan, W.L. Dai and K.N. Fan, Catal. Lett. 88 (2003) 61.
[25] Y.M. Liu, Y. Cao, N. Yi, W.L. Feng, W.L. Dai, S.R. Yan, H.Y. He and K.N. Fan, J. Catal. 224 (2004) 417.
[26] C. Hess, M.H. Looi, S.B. Abd Hamid and R. Schlögl, Chem. Commun. 4 (2006) 451.
[27] S. Jun, S.H. Joo, R. Ryoo, M. Kruk, M. Jaroniec, Z. Liu, T. Ohsuna and O. Terasaki, J. Am. Chem. Soc. 122 (2000) 10712.
[28] R. Ryoo, C.H. Ko, M. Kruk, V. Antochshuk and M. Jaroniec, J. Phys. Chem. B 104 (2000) 11465.
[29] W.E. Slinkard and P.B. Degroot, J. Catal. 68 (1981) 423.
[30] F. Arena, F. Frusteri, G. Martra, S. Coluccia and A. Parmaliana, J. Chem. Soc., Faraday Trans. 93 (1997) 3849.
[31] J. Santamaría-González, J. Luque-Zambrana, J. Mérida-Robles, P. Maireles-Torres, E. Rodríguez-Casllón and A. Jiménez-López, Catal. Lett. 68 (2000) 67.
[32] M.L. Peña, A. Dejoz, V. Fornés, E. Rey, M.I. Vázquez and J.M. López Nieto, Appl. Catal. A 209 (2001) 155.
[33] H. Berndt, A. Martin, A. Brückner, E. Schreier, D. Müller, H. Kosslick, G.U. Wolf and B. Lücke, J. Catal. 191 (2000) 384.
[34] M. Baltes, K. Cassiers, P. Van der Voort, B.M. Weckhuysen, R.A. Schoonheydt and E.F. Vansant, J. Catal. 197 (2001) 160.
[35] A. Brückner, P. Rybarczyk, H. Kosslick, G.U. Wolf and M. Baerns, Stud. Surf. Sci. Catal. 142 (2002) 1141.
[36] T. Blasco, J.M. López Nieto, A. Dejoz and M.I. Vázquez, J. Catal. 157 (1995) 271.